(19) Europäisches Patentamt
European Patent Office
Office européen des brevets

(11) EP 2 255 173 B1

(12) **EUROPEAN PATENT SPECIFICATION**

(45) Date of publication and mention of the grant of the patent:
24.01.2018 Bulletin 2018/04

(21) Application number: **09722309.3**

(22) Date of filing: **18.03.2009**

(51) Int Cl.:
A61B 5/1455 *(2006.01)* ***A61B 5/00*** *(2006.01)*
G01N 21/47 *(2006.01)* ***G01N 21/31*** *(2006.01)*
G06K 9/00 *(2006.01)* ***G06T 7/62*** *(2017.01)*
G06T 7/66 *(2017.01)*

(86) International application number:
PCT/US2009/037511

(87) International publication number:
WO 2009/117485 (24.09.2009 Gazette 2009/39)

(54) **OPTICAL METHOD FOR DETERMINING MORPHOLOGICAL PARAMETERS AND PHYSIOLOGICAL PROPERTIES OF SKIN TISSUE**

OPTISCHES VERFAHREN ZUR FESTLEGUNG MORPHOLOGISCHER PARAMETER UND PHYSIOLOGISCHER EIGENSCHAFTEN VON HAUTGEWEBE

PROCÉDÉ OPTIQUE DE DÉTERMINATION DE PARAMÈTRES MORPHOLOGIQUES ET DE PROPRIÉTÉS PHYSIOLOGIQUES DE TISSU DE PEAU

(84) Designated Contracting States:
AT BE BG CH CY CZ DE DK EE ES FI FR GB GR HR HU IE IS IT LI LT LU LV MC MK MT NL NO PL PT RO SE SI SK TR

(30) Priority: **18.03.2008 US 37503 P**

(43) Date of publication of application:
01.12.2010 Bulletin 2010/48

(60) Divisional application:
15186132.5 / 2 992 818

(73) Proprietor: **Balter, Inc.**
Maplewood, NJ 07040 (US)

(72) Inventors:
- **STAMNES, Jakob, J.**
  N-0382 Oslo (NO)
- **STAMNES, Knut**
  Maplewood, NJ 07040 (US)
- **ZHAO, Lu**
  N-5072 Bergen (NO)
- **HAMRE, Boerge**
  N-5253 Sandsli (NO)
- **RYZHIKOV, Gennady**
  N-5172 Loddefjord (NO)
- **BIRYULINA, Marina**
  N-5172 Loddefjord (NO)
- **SOMMERSTEN, Endre, R.**
  N-5283 Radal (NO)
- **NIELSEN, Kristian, P.**
  DK-6670 Holsted (DK)
- **MOAN, Johan, E.**
  N-0381 Oslo (NO)

(74) Representative: **Hanna Moore + Curley**
Garryard House
25/26 Earlsfort Terrace
Dublin 2, D02 PX51 (IE)

(56) References cited:
WO-A1-2006/076810 **US-A1- 2001 032 053**
US-A1- 2004 030 255 **US-A1- 2004 092 824**
US-A1- 2006 247 532

- **NIELSEN KRISTIAN P. ET AL: "Reflectance Spectra of Pigmented and Nonpigmented Skin in the UV Spectral Region", PHOTOCHEMISTRY AND PHOTOBIOLOGY, vol. 80, no. 3, 1 January 2004 (2004-01-01), pages 450-455, XP55037307, ISSN: 0031-8655, DOI: 10.1562/2004-02-10-RA-079.1**
- **NIELSEN KRISTIAN P. ET AL: "The optics of human skin: aspects important for human health", SOLAR RADIATION AND HUMAN HEALTH, 1 January 2008 (2008-01-01), pages 35-46, XP55001951, Oslo**

Printed by Jouve, 75001 PARIS (FR)

(Cont. next page)

- **NIELSEN K P ET AL: "Retrieval of the physiological state of human skin from UV-Vis reflectance spectra - A feasibility study", JOURNAL OF PHOTOCHEMISTRY AND PHOTOBIOLOGY B: BIOLOGY, ELSEVIER SCIENCE S.A., BASEL, CH, vol. 93, no. 1, 16 October 2008 (2008-10-16), pages 23-31, XP025479324, ISSN: 1011-1344, DOI: 10.1016/J.JPHOTOBIOL.2008.06.010 [retrieved on 2008-07-01]**

Description

BACKGROUND

1. Technical Field

[0001] The present disclosure relates to an optical method for determining several morphological parameters and physiological properties (hereafter abbreviated MP&PPs) of skin tissue. In particular, the present disclosure is directed to a method to determine MP&PPs of malignant as well as benign skin tissue lesions.

2. Description of the Related Art

[0002] Malignant melanoma is one of the most rapidly increasing cancers in the world. In the United States alone, the estimated incidence for 2008 is 62,480, which leads to an estimated total of 8,420 deaths per year. Successful treatment of melanoma depends on early detection by clinicians with subsequent surgical removal of tumors. Visual detection has its limitations, even when augmented with dermoscopy, especially with less experienced users. Attempts have thus been made to develop automated devices to assist in the screening of pigmented skin lesions for likelihood of melanoma. Several of these devices have digitalized dermoscopy-related features analyzed by artificial neural networks or support vector machine learning systems.

[0003] The optical properties of human skin in the ultraviolet spectral region have been studied for almost one hundred years [Hasselbalch, KA: Quantitative Untersuchungen Uber die Absorption der menschlichen Haut von ultravioletten Strahlen. Skand Arch Physiol 1911 25: 5-68, 1911; Everett, MA, Yeargers, E, Sayre, RM, Olson, RL: Penetration of epidermis by ultraviolet rays. Photochem Photobiol 1966 5: 533-542], and non-invasive optical methods have been applied to study the physiological state of human skin for at least twenty years [Diffey, BL, Oliver, RJ, Farr, PM: A portable instrument for quantifying erythema induced by ultraviolet radiation. Br J Dermatol 1984 111: 663-672]. A well-known application is blood-oxymetry, by which a relative blood-oxygenation index can be determined non-invasively from the scattered reflectance or transmittance of light at red and near-infrared (NIR) wavelengths [see e.g. Yaroslavsky AN, Schulze PC, et al. Optical properties of selected native and human brain tissues in vitro in the visible and near infrared spectral range. Physics in Medicine and Biology. 2002 47(12):2059-2073]. The reflectance in that spectral region has also been used to determine other physiological properties. For example, the gradient of the reflectance spectrum between 620 nm and 720 nm depends on the total melanin content of the skin [Kollias N, Baqer AN. Spectroscopic characteristics of human melanin in vivo. J Invest Dermatol, 1985 ;85:38-42], However, variations in the blood concentration, the thicknesses of the skin layers, and the scattering phase function of skin tissue, also affect the reflectance spectrum, and thereby the accuracy of the determination of blood oxygenation and total melanin content. Therefore, it is essential to perform a simultaneous determination of all optically important MP&PPs.

[0004] In order to determine tissue optical properties (as opposed to MP&PPs) from spectral reflectance measurements several different inversion schemes have been used, including partial least squares regression [Berger et al., An enhanced algorithm for linear multivariate calibration, Anal. Chem. 1998, 70: 623-627], neural networks [Kienle et al., Spatially resolved absolute diffuse reflectance measurements for noninvasive determination of the optical scattering and absorption coefficients of biological tissue, Appl. Opt. 35 2304-2314 1996], fuzzy logic [Dam et al., Determination of tissue optical properties from diffuse reflectance profiles by multivariate calibration. Appl Opt. 1998;37:772-778], and genetic algorithms [Zhang et al., "Neural vs. statistical classifier in conjunction with genetic algorithm based feature selection" Pattern recognition letters 26.7 (2005): 909-919]. In contrast, this invention makes use of a nonlinear inversion scheme based on e.g. optimal estimation theory [Tikhonov, A.N., and Arsenin, V.Y., Tikhonov, A. N.; V. Y. Arsenin (1977). Solution of III-posed Problems. Washington: Winston & Sons. ISBN 0-470-99124-01; Twomey, S, Introduction to the Mathematics of Inversion in Remote Sensing and Indirect Measurement Developments in Geomathematics, Vol. 3 Elsevier, Amsterdam (1977); Tarantola, A., Inverse Problem Theory: Methods for Data Fitting and Model Parameter Estimation , Elsevier, New York 1987; Rodgers, Clive D., Inverse Methods for Atmospheric Sounding: Theory and Practice. World Scientific 2000], combined with bio- optical models [which provide a link between MP&PPs and inherent optical properties (IOPs)] and accurate radiative-transfer modeling in coupled air-tissue systems. There is also disclosed, a method for deriving a set of additional morphological parameters (MPs) of tissue from reflectance measurements.

[0005] WO 2006/076810 A1 discloses a method and device for disease detection, more particularly, cancer detection, from the analysis of diffuse reflectance spectra measured in vivo during endoscopic imaging. The measured diffuse reflectance spectra are analyzed using a light-transport model and numerical method to derive quantitative parameters related to tissue physiology and morphology.

[0006] US 2006/247532 A1 discloses an iterative process that calculates the absorption and scattering coefficients of tissue from a set of diffuse reflectance measurements made with an optical spectrometer operating in the UV-VIS spectral range. The relationship between measured diffuse reflectance and the absorption and scattering coefficients is modeled

using a Monte Carlo simulation.

[0007] NIELSEN KRISTIAN P. ET AL: "Reflectance Spectra of Pigmented and Nonpigmented Skin in the UV Spectral Region", PHOTOCHEMISTRY AND PHOTOBIOLOGY, vol. 80, no. 3, 1 January 2004 relates to measurements of reflectance spectra from human skin *in vivo* in the spectral range from 250 to 700 nm. The measured results are simulated using a new radiative transfer model developed to study light propagation in skin tissue.

[0008] NIELSEN KRISTIAN P. ET AL: "The optics of human skin: aspects important for human health", SOLAR RADIATION AND HUMAN HEALTH, 1 January 2008 relates to combining a bio-optical model of human skin with advanced radiative transfer theory to simulate the transport of solar radiation through the skin.

SUMMARY

[0009] The present teaching provides a method as detailed in claim 1. Advantageous features are provided in dependent claims.

BRIEF DESCRIPTION OF THE DRAWINGS

[0010] The objects and features of the present disclosure, which are believed to be novel, are set forth with particularity in the appended claims. The present disclosure, both as to its organization and manner of operation, together with further objectives and advantages, may be best understood by reference to the following description, taken in connection with the accompanying drawings as set forth below:

Figure 1 shows an example of the agreement between measured and simulated reflectance values obtained when using the retrieved values for morphological parameters and physiological properties of the tissue;

Figure 2 shows the retrieved dermal blood concentration for each of the measurement areas;

Figure 3 shows the retrieved percentage of oxygenated blood for each of the measurement areas;

Figure 4 shows retrieved melanosome content in the lower epidermis for each of the measurement areas;

Figure 5 shows retrieved melanosome content in the upper epidermis for each of the measurement areas;

Figure 6 shows retrieved lower epidermis thickness for each of the measurement areas;

Figure 7 shows retrieved upper epidermis thickness for each of the measurement areas; and

Figure 8 shows retrieved epidermal keratin content for each of the measurement areas.

DETAILED DESCRIPTION OF EXEMPLARY EMBODIMENTS

[0011] The following detailed description refers to the accompanying drawings. The same reference numbers in different drawings may identify the same or similar elements. In addition, the following detailed description does not limit the present disclosure. The claimed invention is directed to a method of determining morphological parameters and physiological properties of tissue only insofar as the tissue is skin tissue. Other types of tissue do not fall within the scope of the invention as defined by the claims. The present invention relates to a novel method for determining morphological parameters and physiological properties of the tissue (MP&PPs) of different types of tissue lesions. In particular, the present invention is directed to a method for determining MP&PPs for malignant as well as benign tissue lesions. The method of the present invention is applicable to, but not limited to, benign and malignant tissue lesions in general, and uses spectral reflectance measurements of tissue lesions, which may be generated by a spectrophotometer or by an Optical Transfer Diagnosis (OTD) method.

[0012] The OTD device currently used records 30 spectral reflectance images of a lesion under examination. These 30 reflectance images, which constitute one image set, are recorded at 10 different wavelengths (365-1000 nm) from multiple angles of illumination and detection. According to the invention the OTD device is a spectral reflectance meter consisting of a measurement head with 12 fixed light-emitting diode (LED) lamps and 3 IEEE (Institute of Electrical and Electronics Engineers) 1394 FireWire cameras. Each LED is placed at a different angle relative to the skin to enhance the ability to retrieve information about the depth of the lesion. The polar angles of the LEDs vary between 30 and 45 degrees, and the relative azimuth angles between 34 and 145 degrees. The polar angles of the detectors vary between 0 and 45 degrees, and the relative azimuth angles between 0 and 180 degrees, In the current OTD practice, an alcohol-

based gel is used as an interface between the measurement probe and the skin, and a selected area of the skin is illuminated and imaged through a 2.2 cm diameter circular sapphire plate. The imaging time is approximately 5 seconds.

[0013] On the basis of established absorption and transmission spectra for known tissue chromophores and mathematical modeling of spectral tissue reflectance using a bio-optical model in combination with radiative transfer modeling in coupled air-tissue systems, the present invention provides through the use of a non-linear inversion procedure, a method for deriving MP&PPs as well as additional MPs of a lesion from a set of spectral reflectance measurements. By this method, several MP&PPs can be determined including (i) percentage of hemoglobin; (ii) percentage of hemoglobin oxygenation; (iii) upper epidermal thickness; (iv) lower epidermal thickness; (v) percentage of upper melanosome concentration; (vi) percentage of lower melanosome concentration; and (vii) percentage of keratin concentration. The third and fourth of these entities are MPs, while the remaining five entities are physiological properties (PPs) describing the physiological state of the tissue. Each of these seven entities varies and is different for normal and malignant tissues. Also, the present invention provides a method for deriving a set of additional MPs of diagnostic value directly from the reflectance measurements.

[0014] It is important to combine information about parameters that characterize the physiological state of the skin tissue with information of diagnostic value obtained from MPs other than the thicknesses of the upper and lower epidermis layers. For example, an unusually high melanin content would not suffice to make a definitive melanoma diagnosis, but if a lesion with high melanin content also had an irregular spatial distribution of the reflected intensity, then the high melanin content could indicate with a higher probability that the lesion might be a melanoma.

[0015] To aid the differentiation between benign and malignant tissue, a description of how a lesion can be defined directly from measured reflectance spectra and how such measurements can be used to characterize the lesion in terms of a set of MPs follows. As an example, an aim is to differentiate between benign pigmented nevi and malignant melanomas, but the method is applicable in general to differentiate between benign and malignant tissue.

[0016] A lesion border is defined from measured reflectance spectra by using the reflected intensity from one of the channels in the visible spectral range, for example the green channel. As an example, 10 different MPs are descriptive of the lesion and can be used as an aid to make a definitive diagnosis.

[0017] *Lesion border.* The border of a lesion is defined from the reflected intensity of the image from one of the visible channels, for example the green channel, looking straight down at the lesion, by identifying the regions in which the gradient of the reflected intensity has its largest values.

[0018] Size: The size parameter p_{M1} is defined as the number of pixels comprising the lesion, *i.e.* p_{M1} is the number of pixels inside the lesion border defined above.

[0019] *Histogram width:* For a given combination of illumination and observation directions, the histogram-width parameter p_{M2} gives a measure of the inhomogeneity of the reflected intensity of a lesion. Usually this parameter is small for benign nevi, but large for melanomas. Sebhorreic keratoses can also have relatively large inhomogeneities of the reflected intensity.

[0020] *Relative moment of inertia*: For a given combination of illumination and observation directions, the parameter p_{M3} provides information about another aspect of the inhomogeneity of the reflected intensity of a lesion. Let the spatial light absorptance distribution in a lesion be defined as its "mass distribution" and calculate its "center of mass" and "total mass", the latter being defined as the average light absorptance of the lesion. Then the parameter p_{M3} gives the moment of inertia of the lesion relative to that of a homogeneous circular disk having the same "total mass" as the lesion and a diameter equal to the average diameter of the lesion. If there is a high melanin concentration towards the center of a lesion, this parameter will be small, while it will be large if there is a high melanin concentration towards its border. For the melanomas examined so far, the p_{M3} values were small, in particular for well-developed melanomas.

[0021] *Center distance*: The center distance p_{M4}, which provides additional information about the asymmetry of the lesion, represents the physical distance between the "geometrical center of a lesion" and the "center of mass" of the absorptance, as defined above. The "geometrical center of a lesion" means its center with respect to its border, irrespective of how the pigment is distributed within it. Thus, if a lesion has an asymmetrical pigment distribution, the distance between the "geometrical center" and the "center of mass" will be significant.

[0022] *Darkness*: The darkness parameter p_{M5} is defined as the average value of the reflected intensity of a lesion.

[0023] *Fractal dimension*: The fractal-dimension parameter p_{M6} describes the complexity of the border of a lesion. It is defined such that the border of a lesion has a fractal dimension of 1 if the lesion border is perfectly smooth, independent of magnification, while the fractal dimension of the lesion border will tend towards 2 if it is highly irregular.

[0024] *Asphericity*: The aspericity parameter p_{M7} is defined as the ratio between the long and short axes of a lesion. It is 1 for a circular lesion, and increases as a lesion gets more elongated. Just as p_{M6} and p_{M8}, this parameter depends only on the border of the lesion, and does not contain any information about its internal structure.

[0025] *Relative border length*: The relative border length p_{M8} is defined as the ratio of the border length of a circle with the same area as the lesion to the border length of the lesion.

[0026] *Size vs. fractal dimension*: The parameter p_{M9} is defined as the size divided by the fractal dimension, *i.e.* $p_{M9} = p_{M1} / p_{M6}$.

[0027] *Border length vs. fractal dimension*: The parameter p_{M10} is defined as the relative border length divided by the fractal dimension, *i.e.* $p_{M10} = p_{M8} / p_{M6}$.

[0028] Multi-spectral reflectance measurements combined with bio-optical models and accurate radiative transfer simulations of light propagation inside tissue and backscattering from it, provide a basis for obtaining estimates of MP&PPs. In order to determine important tissue MP&PPs the following ingredients are needed: 1. A bio-optical model that relates tissue MP&PPs to tissue IOPs, the latter being the absorption and scattering coefficients as well as the scattering phase function, each as function of wavelength and depth in the tissue; 2. An accurate radiative transfer model for coupled air-tissue systems. which for a given set of IOPs computes various apparent optical properties (AOPs). such as the diffuse reflectance spectrum; 3. An iterative inversion scheme that accounts for the nonlinear dependence of the AOPs on the IOPs.

[0029] Commonly used radiative transfer models include one based on the diffusion approximation and another based on Monte Carlo (MC) simulations. The first method is not accurate enough for our purpose, and the MC method is too slow. The numerically stable discrete ordinate radiative transfer (DISORT) model provides accurate results for coupled air-tissue systems in an efficient manner. Thus, the DISORT code for coupled air tissue systems (CAT-DISORT) is several orders of magnitude faster than the MC method and provides results that are just as precise. It includes a bio-optical model that has been applied also to provide estimates of the efficiency of various photobiological processes and photodynamic therapy in the UV and visible spectral regions.

[0030] To illustrate the potential of our method for determining tissue MP&PPs, a study was carried out that aimed at evaluating the feasibility of employing the biooptical model together with CAT-DISORT forward simulations and inversion based on Bayesian optimal estimation to determine important MP&PPs of skin tissue from diffuse reflectance spectra measured by Zhao, Y. and Berns, R. S. (2007), Image-based spectral reflectance reconstruction using the matrix R method. Color Res. Appl., 32: 343-351. The biooptical model contains a large number of variable MP&PPs that in principle could be retrieved, but most of them were kept fixed while only a few were treated as
retrievable entities. Chromophores, such as the epidermal melanosome concentration and the dermal blood concentration, were considered as retrievable entities, since their variability strongly influences the apparent optical properties of the tissue, such as the spectral tissue reflectance. But entities describing the optical properties of the cellular matrix into which the chromophores are embedded, were kept fixed because variations in these entities have little impact on the apparent optical properties of the tissue.

[0031] Reflectance spectra in the wavelength region from 300 nm to 600 nm were measured daily from three test areas and three control areas on a volunteer with skin type III for two weeks during which the skin in the test areas went through erythema and pigmentation. The volunteer, who had given his written permission to participate in the study, was healthy and did not use any medical drugs. Erythema and pigmentation were induced after 24-hour topical application of a photosensitizer followed by illumination with red light (632 nm) for 2 minutes on the first day ('day 0') of the experiment. A brief summary of the design of the photodynamic experiment is given below.

[0032] Three test areas (A, B & C), each 1 cm x 1 cm with approximately 1.5 cm distance between adjacent areas, were marked on the inner part of the right forearm of the volunteer. Cream was prepared using 10% (w/w) of the hexylester of 5-aminolevulinic acid (ALA-Hex) in a standard oil-in-water cream base (Unguentum, Merck, Darmstad, Germany). Freshly prepared cream with approximately (75 ± 10) mg/cm^2 of ALA-Hex was topically applied on each of the three test areas, which were subsequently covered with transparent adhesive dressings (OpSite Flexifix, Smith & Nephew Medical Ltd., Hull, UK), in which three openings (1 cm x 1 cm) had been cut out precisely in the places where the test areas were located. The dressings were intended to prevent the cream from diffusing to adjacent areas. The creams and the dressings were kept for 24 hours on the test areas, which were then illuminated with red light (632 nm) for 2 minutes.

[0033] Three control areas, similar to the test areas, were also marked on the volunteer. On the first of these control areas (D) ALA-Hex was applied but it was not illuminated; the second of the control areas (E) was illuminated with red light, but no ALA-Hex was applied; on the third control area (F) a base cream, without ALA-Hex was applied, and it was illuminated with red light.

[0034] A luminescence spectrometer was employed to record reflectance spectra from each of the test areas and each of the control areas. The spectrometer was equipped with two scanning grating monochromators, one in front of the light source (a pulsed Xenon lamp) and another in front of the detector. A fiber-optic probe was coupled to the spectrometer. The probe was a commercially available fiber accessory (Perkin-Elmer), consisting of two 1 m fused silica fiber bundles joined in parallel at the measuring tip. It was connected to a cylindrically shaped aluminum spacer with an inner diameter of 4 mm. The spacer was painted black inside in order to minimize stray light. The spacer was pressed lightly against the skin to keep the probe at a fixed distance of 10 mm above the skin surface. This arrangement ensured a relatively uniform distribution of the excitation light over the area to be examined. Reflectance spectra were measured in synchronous scans in which both gratings were set at the same wavelength and band pass (5 nm) to avoid fluorescence artifacts. The area exposed to the excitation light of the spectrometer was the same as the area from which the reflected light was detected. The geometry of the fiber probe was such that both the directly (Fresnel) reflected and the diffusely reflected irradiances from the skin were collected and recorded. Care was taken not to press the spacer too hard against

the skin surface in order to minimize artifacts from pressure-induced reductions in the blood flow.

[0035] A coupled air-tissue system can be represented by a layered medium with constant inherent optical properties (IOPs) in each layer. The tissue is assumed to be a turbid layered medium so that radiative transfer theory can be used to compute the diffuse light inside it and reflected from it. Each tissue layer can be described in terms of its IOPs, which are the absorption coefficient α([mm^{-1}]), the scattering coefficient σ([mm^{-1}]), the (normalized) scattering phase function $p(\cos\Theta)$, and the physical thickness Δz ([mm]). In terms of α, σ, and Δz, one may define two non-dimensional IOPs given by $\tau=(\alpha+\sigma)\Delta z$ (optical thickness) and $a = \sigma/(\alpha + \sigma)$ (single-scattering albedo), so that the IOPs in each layer of the tissue can be adequately described by the two variables τ and a, as well as a third parameter g, related to the scattering phase function.

[0036] The scattering phase function gives the distribution of the scattered light as a function of the scattering angle Θ. Skin tissue is a complex medium with many different kinds of scattering 'particles' in each layer, and the scattering phase function for a particular layer represents a weighted mean of scattering phase functions for several types of particles. Different descriptions of the scattering phase function $p(\cos\Theta)$ may be used in different physical and practical applications. Here, two such functions, namely the Henyey-Greenstein scattering phase function $p_{HG}(\cos\Theta)$ and the Rayleigh scattering phase function $p_{Ray}(\cos\Theta)$ are used. A convenient measure of the angular distribution of the scattering is the average over all scattering directions (weighted by $p(\cos\Theta)$) of the cosine of the scattering angle Θ, *i.e.* ($\mu = \cos\Theta$)

$$\langle\cos\Theta\rangle = g = \frac{1}{2}\int_0^{\pi} p(\cos\Theta)\cos\Theta\sin\Theta\, d\Theta = \frac{1}{2}\int_{-1}^{1} p(\mu)\mu\, d\mu. \qquad (1)$$

The average cosine g is called the *asymmetry factor* of the scattering phase function.

[0037] In 1941 Henyey and Greenstein proposed the one-parameter scattering phase function given by

$$p_{HG}(\cos\Theta) = \frac{1-g^2}{(1+g^2-2g\cos\Theta)^{3/2}} \qquad (2)$$

where g is the asymmetry factor [see Eq. (1)]. This Henyey-Greenstein scattering phase function has no physical basis, but is useful for describing scattering by large particles in a medium, such as tissue, for which the actual scattering phase function is unknown. Here, the term 'large particles' implies that their sizes are comparable to or larger than the wavelength. When the size d of the scatterers is small compared with the wavelength of light $(d < \frac{1}{10}\lambda)$, the Rayleigh scattering phase function gives a good description of the angular distribution of the scattered light. The Rayleigh scattering phase function for unpolarized light is given by

$$p(\cos\Theta) = \frac{3}{4+f}(1 + f\cos^2\Theta) \qquad (3)$$

where f is a polarization factor. Originally, the Rayleigh scattering phase function was derived for scattering of light by an electric dipole. Since the Rayleigh scattering phase function is symmetric about $\Theta = 90°$, the asymmetry factor is $g = 0$. However, unlike the Heney-Greenstein scattering phase function [Eq. (2)], which gives isotropic scattering for $g = 0$, the Rayleigh scattering phase function does not represent isotropic scattering.

[0038] A bio-optical model was used to calculate the IOPs for a given set of MP&PPs that describe the physiological state of the tissue. In order to calculate the AOPs (in this case the diffuse reflectance spectrum from the tissue), the CAT-DISORT was employed to solve the radiative transfer equation for a slab of biological tissue stratified into a number of layers, thereby accounting for the reflection and refraction of the incident radiance at the air-tissue interface (caused by the change in the refractive index), which affect the radiation field significantly. An integral part of the forward-inverse modeling procedure was to couple the bio-optical model to CAT-DISORT in such a way that the MP&PPs could be determined directly from the measured AOPs.

[0039] In order to obtain a unique solution of our inverse or retrieval problem, most MP&PPs are kept fixed, while other MP&PPs are considered to be retrievable, and therefore allowed to vary. The following 7 retrievable MP&PPs varied:

- The dermal blood content
- The percentage of oxygenated blood

- The melanosome concentration in the lower epidermis
- The thickness of the lower epidermis
- The melanosome concentration in the upper epidermis
- The thickness of the upper epidermis
- The keratin concentration in the upper epidermis.

[0040] The other MP&PPs were fixed. Thus, each of the scattering coefficients associated with the non-pigmented constituents of the epidermis and the dermis, the optical thickness of the dermis, and the optical properties of the subcutaneous layer were assumed to be fixed.

[0041] Figure 1 shows an example of the agreement between measured and simulated reflectance values obtained when using the retrieved values for the 7 MP&PP entities listed above as inputs to CAT-DISORT simulations. In Figure 1, measured (+) and simulated (x) reflectance spectra for test area A on the seventh day after the photodynamic exposure is shown. The figure shows that good agreement was obtained between measured and simulated spectra when the 7 retrieved MP&PPs for this day were used as inputs to CAT-DISORT simulations.

[0042] Figures 2-8 show the retrieved values of the blood content in the dermis (Fig. 2), the percentage of oxygenated blood (Fig 3), the melanosome concentration in the lower layer of the epidermis (Fig. 4), the melanosome concentration in the upper layer of the epidermis (Fig. 5), the thickness of the lower epidermis (Fig. 6), the thickness of the upper epidermis (Fig. 7), and the keratin concentration in the upper epidermis (Fig. 8), respectively. The three panels in the left column of each figure represent the test areas (A-C), while the three panels in the right column represent the control areas (D-F). In the bio-optical model for tissue the epidermis was divided into five layers and the melanosome concentration was allowed to vary from one layer to another. Here, the epidermis is divided into two layers and the melanosome concentration and the thickness for each of them are retrieved.

[0043] In Figure 2, retrieved dermal blood concentration for each of the measurement areas for the 15 days of measurement is shown. 'Initial' refers to the situation prior to the photodynamic treatment of the skin, while the next tick mark refers to the situation immediately after the photodynamic treatment.

[0044] In Figure 3, retrieved percentage of oxygenated blood for each of the measurement areas for the 15 days of measurement is shown. 'Initial' refers to the situation prior to the photodynamic treatment of the skin, while the next tick mark refers to the situation immediately after the photodynamic treatment.

[0045] In Figure 4, retrieved melanosome content in the lower epidermis for each of the measurement areas for the 15 days of measurement is shown. 'Initial' refers to the situation prior to the photodynamic treatment of the skin, while the next tick mark refers to the situation immediately after the photodynamic treatment.

[0046] In Figure 5, retrieved melanosome content in the upper epidermis for each of the measurement areas for the 15 days of measuremen is shown. 'Initial' refers to the situation prior to the photodynamic treatment of the skin, while the next tick mark refers to the situation immediately after the photodynamic treatment.

[0047] In Figure 6, retrieved lower epidermis thickness for each of the measurement areas for the 15 days of measuremen is shown. 'Initial' refers to the situation prior to the photodynamic treatment of the skin, while the next tick mark refers to the situation immediately after the photodynamic treatment.

[0048] In Figure 7, retrieved upper epidermis thickness for each of the measurement areas for the 15 days of measurement is shown. 'Initial' refers to the situation prior to the photodynamic treatment of the skin, while the next tick mark refers to the situation immediately after the photodynamic treatment.

[0049] In Figure 8, retrieved epidermal keratin content for each of the measurement areas for the 15 days of measurement is shown. 'Initial' refers to the situation prior to the photodynamic treatment of the skin, while the next tick mark refers to the situation immediately after the photodynamic treatment.

[0050] The standard deviations or the error bars that are shown in Figs. 2-8 were calculated during the retrieval procedure from the diagonal elements of the covariance matrix $[\Phi_{final}]^{-1}$ as defined in Eq. (19) below and explained in the discussion that follows Eq. (19). In general, the temporal variation in the blood content of the tissue (Fig. 2) was in good agreement with expectations. A maximum was reached after 1-2 days, the so-called erythema reaction, typical for sunburn, after which the blood content slowly decayed. This pattern is similar for the three test areas. For the three control areas the variations are within the range of the calculated standard deviations.

[0051] Fig. 3 shows the percentage of oxygenated blood immediately after the photodynamic treatment and during the following two weeks for the six measurement areas. Photodynamic therapy is known to be an oxygen consuming process. Thus, it must be emphasized that 'immediately after' means several seconds or may be even a minute after the exposure. The marked increase in oxygenation measured at the beginning of the experiment, at all the three test areas, is likely to be a reaction to the photodynamic treatment, rather than a direct effect of the treatment itself. The variation in blood oxygenation at the three control areas is of a stochastic nature.

[0052] The relative change of the percentage of oxygenated blood during the two weeks of measurements seems reasonable. However, the absolute values, which are in the range between 40% and 80%, may be too low (Fig. 3). These low oxygenation percentages could be caused by the bandpass of the spectrometer (5 nm) being insufficiently

narrow to resolve the spectral fine structure in the 540 nm - 580 nm spectral region. The skin reflectance in this spectral region is very sensitive to the percentage of oxygenated blood. Therefore, the percentage of oxygenated blood could be underestimated from these measurements.

[0053] The retrieval of the melanosome content was less uncertain for the upper epidermis (Fig. 5) than for the lower epidermis (Fig. 4). Thus, the standard deviations for the lower epidermal melanosome content were about twice as large as for the upper epidermal melanosome content.

[0054] For the three test areas, the melanosome content in the lower epidermis decreased during the two weeks (Fig. 4), while the melanosome content in the upper epidermal layer increased, in particular during the first week (Fig. 5). This behaviour is similar to that caused by pigmentation induced by UVB radiation (with wavelengths shorter than 320 nm). Thus, as a reaction to UVB exposure the melanosome pigment particles tend to be transferred from the melanocytes in the basal layer of the epidermis to the keratinocytes in the upper layer. In the experiment discussed here, there was no sign of immediate pigment darkening, a process primarily induced by UVA radiation (with wavelengths longer than 320 nm). Had immediate pigment darkening occurred, it would have been seen in the measurements taken immediately after the photodynamic treatment.

[0055] Hence, the photodynamic process induced by topical application of ALA-Hex followed by illumination with red light (632 nm wavelength) bears similarities with the photobiological pigmentation process induced by UVB radiation, but immediate melanin darkening does not take place during PDT.

[0056] The decrease in the retrieved lower melanosome concentration occurs simultaneously with an increase in the retrieved lower epidermal thickness. Thus, the total retrieved lower epidermal melanosome content turned out to b~ fairly constant during the two weeks of measurements. No significant temporal variations were found in the control areas in either the retrieved lower or upper epidermal melanosome concentrations (Figs. 4 & 5) or in the retrieved lower or upper epidermal thickness (Figs. 6 & 7).

[0057] The retrieved thickness of the total epidermis is close to what would be expected. Thus, Sandby-Møller et al., Epidermal Thickness at Different Body Sites: Relationship to Age, Gender, Pigmentation, Blood Content, Skin Type and Smoking Habits, Acta Derm Venereol 2003; 83: 410-413 (2003) performed measurements on the dorsal forearm of 71 volunteers and found the average epidermal thickness to be 76 μm $\pm$ 15 μm. As can be seen from Figs. 6 & 7, a total epidermal thickness of approximately 70 μm for both the test sites and the control sites was retrieved. Thus, the epidermal thickness appears to be retrieved well from the measurements.

[0058] It is feasible to perform accurate retrievals of several key MP&PPs describing the physiological state of human skin tissue by using an accurate radiative transfer model for the coupled air-tissue system as a forward model in conjunction with a bio-optical model and a nonlinear inversion scheme.

[0059] Retrievals made from analyses of diffuse reflectance spectra measured before and after the exposure of the skin to ALA-Hex photodynamic treatment (PDT) with red light, and on each day for two weeks after that PDT exposure provided results in good agreement with those obtained in previous investigations of UVB-induced erythema and pigmentation in human skin:

- The erythema maximizes 1-2 days after the ALA-Hex PDT exposure and then subsides;
- There is a strong increase in the pigmentation of the upper epidermal layers, in particularly during the first 7 days after the ALA-Hex PDT exposure;
- The blood oxygenation is found to increase immediately after the exposure and then return to pre-exposure values more than seven days later.

[0060] The process induced in the skin by ALA-Hex PDT with red light thus appears to be similar to the process induced by UVB radiation.

[0061] These results represent the first simultaneous quantitative retrievals of the melanosome concentrations in the upper and the lower epidermis, the epidermal keratin concentration, the dermal blood concentration, and the percentage of oxygenated blood.

[0062] In a forward model, an assumption may be made that tissue may be modeled as a turbid, plane-parallel, vertically inhomogeneous, layered medium with specified optical properties. Thus, the inherent optical properties (IOPs), i.e., the absorption coefficient $\alpha(z)$, the scattering coefficient $\sigma(z)$ and the normalized scattering phase function $p(z,\Theta)$ were allowed to vary with depth z in the tissue. Here, Θ is the scattering angle, and the differential optical depth for a thin layer of thickness dz is $d\tau = -(\alpha(z) + \sigma(z))dz$. Lateral variations in the IOPs may be ignored, keeping in mind that every measured value corresponds to the radiance reflected by the tissue into the upper hemisphere and then gathered by the finite aperture of an optical system.

[0063] The integro-differential equation of radiative transfer describing light propagation in such a medium can be written in the form:

$$u\frac{dI(\tau,u,\phi)}{d\tau} = I(\tau,u,\phi) - J(\tau,u,\phi) \tag{4}$$

where the source function is given by

$$J(\tau,u,\phi) = \frac{a(\tau)}{4\pi}\int_0^{2\pi} d\phi' \int_{-1}^{1} du'\, p(\tau,u,\phi;u',\phi')I(\tau,u',\phi') + Q(\tau,u,\phi). \tag{5}$$

[0064] Here $I(\tau,u,\phi)$ stands for the diffuse radiance, u is the cosine of the polar angle θ, and ϕ is the azimuth angle. The angles (θ',ϕ') denote the direction of a beam of light before a scattering event and the angles (θ,ϕ) denote the observation direction. The scattering angle Θ between these two directions is given by
$\cos\Theta = \cos\theta\cos\theta' + \sin\theta\sin\theta'\cos(\theta' - \phi)$.

[0065] The first term in the source function $J(\tau,u,\phi)$ represents multiple scattering, $a(\tau) = \sigma(\tau)/[\alpha(\tau) + \sigma(\tau)]$ denotes the single-scattering albedo, and

$$Q(\tau,u,\phi) = \frac{a(\tau)}{4\pi} p(\tau,u,\phi;-\mu_0,\phi_0)S_b(\tau)\exp(-\tau/\mu_0) \tag{6}$$

describes the incident beam of irradiance S_b in direction $(-\mu_0,\phi_0)$ with $\mu_0 \equiv \cos\theta_0$, where θ_0 is the polar angle of the incident beam. The probability of scattering an angle Θ from the direction (θ',ϕ') into the direction (θ,ϕ) is described by the scattering phase function $p(\tau,\cos\Theta) = p(\tau,u,\phi;u',\phi')$, whose first moment or asymmetry parameter, is given by ($\mu = \cos\Theta$) $g(\tau) = \frac{1}{2}\int_{-1}^{1} \mu p(\tau,\mu)d\mu$, as ih Eq. (1). To quantify the propagation of UV and visible light in a turbid layered medium with known IOPs, as well as the diffuse reflectance spectra (apparent optical properties: AOPs), the CAT-DISORT (**C**oupled **A**ir-**T**issue **DIS**crete- **O**rdinate **R**adiative **T**ransfer) model is used to solve Eq. (4). Thus, the IOPs were used as input to the CAT-DISORT model to compute the reflected radiances (AOPs) in directions (θ_a,ϕ_a) inside the detector aperture. To simulate measurement values the computed radiances were integrated over the solid angle $(\Delta u_a,\Delta\phi_a)$ of the optical system aperture. In other words, CAT-DISORT was used to solve the forward problem: for given IOPs of the layered tissue: $g(\tau) = \{\alpha(\tau),\sigma(\tau),g(\tau)\}$, predict (simulate) values for the diffuse reflectance spectra (AOPs): $\tilde{\mathbf{f}} = \{\tilde{f}_1,\tilde{f}_2,\ldots,\tilde{f}_n,\ldots\tilde{f}_N\}$. where $\tilde{f}_n$ (n = 1,2,...N) corresponds to the reflected radiance at N different wavelengths, and $\tilde{f}_n = \tilde{f}_n(g) = \int_{\Delta\phi 4} d\phi_a \int_{\Delta u 6} du_a I_n(0,u_a,\phi_a)$.

[0066] Simulated data $\tilde{\mathbf{f}}$ differ from measured data **f** because the latter contain a stochastic component $\vec{\varepsilon}$, i.e. *noise,* so that

$$\mathbf{f} = \tilde{\mathbf{f}}(\mathbf{g}) + \vec{\varepsilon}\,. \tag{7}$$

[0067] The covariance matrix of the noise $C_\varepsilon = \mathbf{E}\{\vec{\varepsilon}\,\vec{\varepsilon}^{\,T}\}$ is estimated, where **E** is the *mathematical expectation operator.* The superscript ^{T} means *transposition,* so that if $\vec{\varepsilon}$ denotes a *column vector,* $\vec{\varepsilon}^{\,T}$ is the corresponding *row vector,* and thus $\vec{\varepsilon}\,\vec{\varepsilon}^{\,T}$ is a symmetric matrix of dimension $N \times N$.

[0068] In formulation of an inverse problem, note that the tissue IOPs assembled in the vector g depend on the wavelength of the incident light. Second, tissue model parameters are assembled in a vector s. Thus:

$$\mathbf{s} = \{s_1, s_2, \ldots, s_m, \ldots, s_M\}$$

represents M issue MP&PP components (such as the contents of melanosomes, blood, keratin, etc. in the tissue layers). Provided that the spectral signatures of all MP&PP components are known, they can be used to define the IOPs of the tissue:

$$\mathbf{g} = \mathbf{g}(\mathbf{s}).$$

[0069] Letting *F* denote a nonlinear operator that maps a vector of MP&PP tissue components into a vector of simulated measurements, i.e. $\tilde{f}(g) = F(s)$, the model can be rewritten

$$\mathbf{f} = F(\mathbf{s}) + \vec{\varepsilon} \quad (8)$$

[0070] Note that the operator *F* is defined implicitly. It returns a solution of the radiative transfer Eq. (4) for the layered medium with IOPs g, induced by tissue parameters s : g = g(s) and known incident beam S_b.

[0071] Now, an inverse problem is presented: given *N* spectral reflectance measurements with a certain level of noise $(\vec{\varepsilon})$: $\mathbf{f} = F(\mathbf{s}) + \vec{\varepsilon}$, find *M* parameters *s*, which describe the optically important MP&PP components of the tissue.

[0072] Even though the number of measurements *N* is much greater than the number of unknowns *M*, the inverse problem is still underdetermined (ill-posed). The reason for the ill-posedness is the smoothness of most of the spectral signatures of the MP&PP tissue components, implying that the spectral signature of one MP&PP component can be mimicked by a certain combination of others. This makes it hard if not impossible to find the proper impact of an individual MP&PP component, if the parameterization of the tissue model in terms of MP&PP components is done without proper analysis of the information content.

[0073] To alleviate this problem, a regularization procedure may be invoked. Because the data for the inverse problem contain stochastic noise, Bayesian inference provides a natural way of regularization through the introduction of a probabilistic measure in the space of unknown parameters. From Bayes' theorem on conditional probabilities

$$p(\mathbf{f}\,|\,\mathbf{s})p(\mathbf{s}) = p(\mathbf{s}\,|\,\mathbf{f})p(\mathbf{f})$$

it follows that the conditional probability p(**s**|**f**) to get a specific value **s,** when **f** is given, can be written as

$$p(\mathbf{s}\,|\,\mathbf{f}) \propto p(\mathbf{f}\,|\,\mathbf{s})\,p(\mathbf{s}).$$

[0074] If a set of admissible functions {**s**} is defined by the mean value $\mathbf{s_0} = E\{\mathbf{s}\}$, and the covariance matrix $C_s = E\{(\mathbf{s} - \mathbf{s_0})(\mathbf{s} - \mathbf{s_0})^T\}$, then the conditional probability can be represented by the product of two Gaussian distributions. The first one is Gaussian with respect to the noise $\vec{\varepsilon} = \tilde{\mathbf{f}} - \mathbf{f}$, but not with respect to the MP&PP components **s,** because $\vec{\varepsilon} = \mathbf{f} - F(\mathbf{s})$ contains the nonlinear function *F*(**s**). Thus:

$$p(\mathbf{s}\,|\,\mathbf{f}) \propto \exp\{-\frac{1}{2}[\mathbf{f} - F(\mathbf{s})]^T \mathbf{C}_\varepsilon^{-1}[\mathbf{f} - F(\mathbf{s})]\} \times \exp\{-\frac{1}{2}(\mathbf{s} - \mathbf{s_0})^T \mathbf{C}_s^{-1}(\mathbf{s} - \mathbf{s_0})\} = \exp\{-\frac{1}{2}J(\mathbf{s})\}. \quad (9)$$

[0075] If we define the solution **s*** as the vector of most probable tissue components, given the vector of measurement **f**, i.e. $p(\mathbf{s}^*|\mathbf{f}) = \max_s p(\mathbf{s}|\mathbf{f})$, then the solution to the inverse problem can be formulated as an optimization: *find* the vector **s*** from a set of admissible vectors {s} that yields the optimum (*minimum*) value of the functional

$$J = J(\mathbf{s}) = [\mathbf{f} - F(\mathbf{s})]^T \mathbf{C}_\varepsilon^{-1}\,[F(\mathbf{s}) - \mathbf{f}]\}\,[\mathbf{f} - F(\mathbf{s})] + (\mathbf{s} - \mathbf{s_0})^T \mathbf{C}_s^{-1}(\mathbf{s} - \mathbf{s_0}). \quad (10)$$

[0076] Thus, the functional in Eq. (10) (objective function) is the weighted least mean squares difference between simulated and measured radiances, with an extra regularization term (penalty function), represented by the second term in Eq. (10), which is strictly convex and defines the set of admissible tissue component parameters.

[0077] An outline of the Gauss-Newton algorithm for nonlinear inversion is now presented. The objective function in

Eq. (10) near the reference model $\mathbf{s_0}$ in terms of $\bar{\mathbf{s}} = \mathbf{s} - \mathbf{s_0}$:

$$J(\mathbf{s}) = J(\mathbf{s}_0 + \tilde{\mathbf{s}}) = J(\mathbf{s}_0) + \Delta J(\tilde{\mathbf{s}}) = const + \Delta J(\tilde{\mathbf{s}}). \tag{11}$$

[0078] Assuming that $|\bar{\mathbf{s}}| \ll |\mathbf{s_0}|$, an approximate the term $\Delta J(\bar{\mathbf{s}})$ in Eq. (10) by a quadratic form with respect to $\bar{\mathbf{s}}$. Thus, keeping just the constant and the linear term of $F(\mathbf{s})$, is

$$F(\mathbf{s}) = \mathbf{F}(\mathbf{s}_0) + \frac{\partial \mathbf{F}}{\partial \mathbf{s}}|_{\mathbf{s}_0}\,\tilde{\mathbf{s}} + \ldots \equiv \mathbf{F}(\mathbf{s}_0) + \mathbf{L}_o\,\tilde{\mathbf{s}} + \ldots \approx \mathbf{F}(\mathbf{s}_0) + \mathbf{L}_o\,\tilde{\mathbf{s}}. \tag{12}$$

[0079] Here the linear operator $\mathbf{L}_o$ stands for the Jacobian

$$\mathbf{L}_o = \frac{\partial F}{\partial \mathbf{s}}|_{\mathbf{s}_0} = \frac{\partial \tilde{\mathbf{f}}}{\partial \mathbf{g}}\frac{\partial \mathbf{g}}{\partial \mathbf{s}}|_{\mathbf{s}_0} \tag{13}$$

where the subscript indicates that the reference state $\mathbf{s_0}$ is used to evaluate the Jacobian (Frèchet derivative). Similarly, $\mathbf{L}_i$ is used for the Frèchet derivatives evaluated at state $\mathbf{s}_i$.

[0080] The linear approximation in Eq. (12) corresponds to approximating the conditional probability (9) with a Gaussian distribution of unknowns $\mathbf{s}$:

$$p(\mathbf{s}\,|\,\mathbf{f}) \propto \exp\{-\frac{1}{2}J(\mathbf{s}_0)\}\exp\{-\frac{1}{2}\Delta J(\tilde{\mathbf{s}})\propto \exp\{-\frac{1}{2}\Delta J(\tilde{\mathbf{s}})\}$$

which can be approximated as

$$p(\mathbf{s}\,|\,\mathbf{f}) \propto \exp\{-\frac{1}{2}[(\mathbf{L}_o\,\tilde{\mathbf{s}} - \delta\,\mathbf{f})^T\,\mathbf{C}_\varepsilon^{-1}\,(\mathbf{L}_o\,\tilde{\mathbf{s}} - \delta\,\mathbf{f}) + \tilde{\mathbf{s}}^T\,\mathbf{C}_s^{-1}\,\tilde{\mathbf{s}}]\} \tag{14}$$

with $\delta\,\mathbf{f} = \mathbf{f} - F(\mathbf{s}_0)$. It is easy to check that

$$(\mathbf{L}_o\,\tilde{\mathbf{s}} - \delta\,\mathbf{f})^T\,\mathbf{C}_\varepsilon^{-1}\,(\mathbf{L}_o\,\tilde{\mathbf{s}} - \delta\,\mathbf{f}) + \tilde{\mathbf{s}}^T\,\mathbf{C}_s^{-1}\,\tilde{\mathbf{s}} \equiv (\tilde{\mathbf{s}} - \tilde{\mathbf{s}}^*)^T\,\Phi_o\,(\tilde{\mathbf{s}} - \tilde{\mathbf{s}}^*) + \Delta(\mathbf{f}) \tag{15}$$

where $\Delta(\mathbf{f})$ is a term that depends only on the data ($\mathbf{f}$),

$$\mathbf{s}^* = \Phi_o^{-1}\,\mathbf{L}_o^T\,\mathbf{C}_\varepsilon^{-1}\,(\mathbf{f} - F(\mathbf{s}_0)) \tag{16}$$

and

$$\Phi_o = \mathbf{L}_o^T\,\mathbf{C}_\varepsilon^{-1}\,\mathbf{L}_o + \mathbf{C}_s^{-1}. \tag{17}$$

[0081] Using Eq. (15), we get for the conditional probability in Eq. (14):

$$p(\tilde{\mathbf{s}}\,|\,\mathbf{f}) \propto \exp[-\frac{1}{2}(\tilde{\mathbf{s}} - \tilde{\mathbf{s}}^*)^T\,\Phi_o\,(\tilde{\mathbf{s}} - \tilde{\mathbf{s}}^*) \tag{18}$$

which now has the standard form of a Gaussian distribution with the following parameters: the mean value $\mathbf{E}\{\tilde{\mathbf{s}}\} = \tilde{\mathbf{s}}^*$ (which is the same as the most probable one: $\max \mathrm{p}(\tilde{\mathbf{s}} \mid \mathbf{f}) = \mathrm{p}(\tilde{\mathbf{s}}^* \mid \mathbf{f})$), and the covariance matrix

$$\mathbf{E}\{(\tilde{\mathbf{s}} - \tilde{\mathbf{s}}^*)(\tilde{\mathbf{s}} - \tilde{\mathbf{s}}^*)^T\} = [\Phi_o]^{-1} = [\mathbf{L}_o^T \mathbf{C}_\varepsilon^{-1} \mathbf{L}_o + \mathbf{C}_s^{-1}]^{-1}. \quad (19)$$

[0082] Hence, Eq. (16) provides an explicit form of the solution **s*.** Thus, no matter which specific algorithms one applies to solve the linearized version of the optimization problem (11), one should arrive at the solution given by Eq. (16) with uncertainties given by Eq. (19).

[0083] As soon as **s*** is obtained, the corrected reference model becomes

$$\mathbf{s}_1 = \mathbf{s}_0 + \mathbf{s}^*$$

and the procedure can be repeated with models $\mathbf{s}_1$, $\mathbf{s}_2$, ..., until the misfit between simulated and measured data reaches the level of the noise in the data.

[0084] The uncertainties in the final solution are given by covariance matrix $[\Phi_{final}]^{-1}$, and the diagonal elements of this matrix give us an estimate of the dispersions of the corresponding tissue model components.

[0085] In defining a lesion, the morphological image analysis is based on the logarithm of the measured bidirectional reflectance distribution function ρ, defined as:

$$\rho = \ln\left(\frac{L_r}{F_i}\right) \quad (20)$$

where L_r is the reflected intensity or radiance and F_i is the incident lamp flux or irradiance.

[0086] The computed morphological parameters are defined as follows:

Lesion border: The border of a lesion is defined from the reflected intensity of the image from one of the visible channels, for example the green channel, looking straight down on the lesion, by identifying the regions in which the gradient of the reflected intensity has its largest values.

Size: The size parameter p_{M1} is defined as the number of pixels comprising the lesion, i.e. p_{M1} the number of pixels inside the lesion border defined above.

Histogram width: Let $h(\rho)$ be the number of pixels having reflectance values between ρ and $\rho+\Delta\rho$. We then define the width parameter p_{M2} of the lesion histogram as

$$p_{M2} = \frac{1}{H}\int_{-\infty}^{\rho_t} h(\rho)\sqrt{(\rho - \bar{\rho})^2}\, d\rho \quad (21)$$

where ρ_t defines the lesion border, and $H = \int_{-\infty}^{\rho_t} h(\rho)d\rho$, $\bar{\rho} = \frac{1}{H}\int_{-\infty}^{\rho_t} \rho h(\rho)d\rho$.

[0087] Moment of inertia: The "center of mass" of a lesion is

$$\mathbf{r}_M = \frac{\sum_{ij} \rho_{ij}\mathbf{r}_{ij}}{\sum_{ij} \rho_{ij}} \quad (22)$$

where the subscripts i and *j* denote pixel number *i* in the *x* direction and number *j* in the *y* direction, and $\mathbf{r}_{ij}$ is the vector $\mathbf{r}_{ij} = i\hat{\mathbf{e}}_\mathbf{x} + j\hat{\mathbf{e}}_\mathbf{y}$. The moment of inertia for rotation around the *z* axis is given by

$$M_z = \frac{1}{N}\sum_{ij}\rho_{ij}(\mathbf{r}_{ij}-\mathbf{r}_M)^T(\mathbf{r}_{ij}-\mathbf{r}_M) \tag{23}$$

where N is the number of pixels and the superscript T denotes the transpose. Let h_c and r_c be defined as respectively the height and radius of a cylinder with the same "volume" $V = \int_A \rho da$ and area A as the lesion, so that

$$h_c = \frac{V}{\pi r_c^2} \qquad r_c = \sqrt{\frac{A}{\pi}}. \tag{24}$$

[0088] Then, the moment of inertia parameter is defined as

$$p_{M3} = \frac{M_z}{\frac{1}{2}\pi h_c r_c^4} \tag{25}$$

where the denominator is the moment of inertia of the cylinder of radius r_c and height h_c for rotation around its axis. M_z is defined in Eq. (23).

[0089] Center distance: Let $a_{ij} = 1$ for all $\rho_{ij} < 0$ and $a_{ij} = 0$ for all $\rho_{ij} = 0$ (Note that ρ is zero outside the lesion.). "Geometrical center" of the lesion as

$$\mathbf{r}_A = \frac{\sum_{ij} a_{ij}\mathbf{r}_{ij}}{\sum_{ij} a_{ij}}. \tag{26}$$

[0090] The center distance of the lesion is defined as the distance between the "center of mass" of the lesion [Eq. (22)] and the "geometrical center" of the lesion divided by the radius r_c of the cylinder, i.e.

$$p_{M4} = \frac{|\mathbf{r}_M - \mathbf{r}_A|}{r_c}. \tag{27}$$

[0091] Darkness: The darkness parameter is defined as the average value of ρ

$$p_{M5} = \frac{\sum_{ij}\rho_{ij}}{\sum_{ij} a_{ij}} \tag{28}$$

where a_{ij} is equal to 1 inside the lesion and equal to 0 outside it.

[0092] Fractal dimension: The fractal dimension parameter p_{M6} is defined as

$$p_{M6} = \frac{\ln\alpha - \ln N_b}{\ln s} \tag{29}$$

where N_b is the number of lesion border pixels and s is the pixel size, and α is found by a linear fit to the varying values of $\ln N_b$ and $\ln s$ obtained from successive runs with varying resolution. p_{M6} takes values between 1 and 2 depending on the curliness of the lesion border.

[0093] Asphericity: The eigenvalues λ_1 and λ_2 of the following matrix give the moment of inertia around the two principal axes of the lesion.

$$M = \frac{1}{N}\sum_{ij}\rho_{ij}(\mathbf{r}_{ij} - \mathbf{r}_V)(\mathbf{r}_{ij} - \mathbf{r}_V)^T. \quad (30)$$

[0094] Asphericity of the lesion is

$$p_{M7} = \frac{\lambda_1}{\lambda_2}. \quad (31)$$

[0095] Border length: The border length of a lesion is defined as the ratio of the border length of a circle with the same area as the lesion to the border length of the lesion:

$$p_{M8} = \frac{2\sqrt{\pi p_{M1}}}{N_b} \quad (32)$$

where p_{M1} is the size of the lesion and N_b is the number of border pixels.

[0096] Size vs. fractal dimension: The parameter p_{M9} is defined as the size dived by the fractal dimension, i.e. $p_{M9} = p_{M1} / p_{M6}$.

[0097] Border length vs. fractal dimension: The parameter p_{M10} is defined as the relative border length dived by the fractal dimension, i.e. $p_{M10} = p_{M8} / p_{M6}$.

[0098] Morphology Diagnostic Index for Melanoma: a diagnostic index I_{Mk} for each of the morphological parameters p_{Mk} is

$$I_{Mk} = \frac{\ln p_{Mk} - \mu_{Mk}}{\sigma_{Mk}} \quad (33)$$

where μ_{Mk} and σ_{Mk} are the mean value and the standard deviation of $\ln p_{Mk}$ for all lesions under consideration.

[0099] No element, act, or instruction used in the present disclosure should be construed as critical or essential unless explicitly described as such. In addition, as used herein, the article "a" is intended to include one or more items. Where only one item is intended, the term "one" or similar language is used.

[0100] It will be understood that various modifications may be made to the embodiments disclosed herein. Therefore, the above description should not be construed as limiting, but merely as exemplifications of the various embodiments of the present disclosure. Those skilled in the art will envision other modifications within the spirit of the claims appended hereto.

Claims

1. An optical method for determining morphological parameters and physiological properties of skin tissue, the method comprising the steps of:

   generating reflectance measurements of a skin tissue area from reflectance images obtained for a plurality of wavelengths from multiple angles of illumination and detection using a spectral reflectance meter consisting of a measurement head with 12 fixed light-emitting diode (LED) lamps and 3 cameras, wherein each LED lamp is placed at a different angle relative to the skin, providing a bio-optical model, a radiative transfer model, and a non-linear inversion procedure;
   systematically varying input values of the morphological parameters and physiological properties of the skin tissue and simultaneously varying inherent optical properties of the skin tissue, wherein the inherent optical properties are linked to the morphological parameters and the physiological properties of the skin tissue by the bio-optical model, and computing reflectances by the radiative transfer model for the varying inherent optical properties until an agreement between the reflectance measurements and the reflectances computed by the radiative transfer model reaches a predetermined level of accuracy; and
   obtaining the morphological parameters and the physiological properties returned by the non-linear inversion procedure.

2. The method of claim 1, wherein the bio-optical model is based on established absorption and transmission spectra for known skin tissue chromophores and relates morphological parameters and physiological properties of tissue to inherent optical properties of tissue.

3. The method of claim 1, wherein the radiative transfer model is used in coupled air-tissue systems to compute synthetic reflectance spectra for a plurality of different wavelengths and a plurality of different measurement configurations, each with specified directions of illumination and observation.

4. The method of claim 1, wherein the non-linear inversion procedure is based on an optimal estimation theory to solve the inverse problem of quantifying specified morphological parameters and physiological properties of skin tissue, the morphological parameters and physiological properties of skin tissue optionally including, dermal blood content, percentage blood oxygenation, upper epidermis thickness, lower epidermis thickness, percentage of upper melanosome concentration, percentage of lower melanosome concentration, and percentage of keratin concentration.

5. The method of claim 1, wherein the method is used to discriminate between one of:

benign pigmented lesions and malignant melanoma;
benign tissue and basal cell carcinoma; and
benign tissue and squamous cell carcinoma.

6. The method of claim 1, wherein the method is used for beauty care, forensic medicine, or to monitor efficacies of different kinds of treatment.

Patentansprüche

1. Optisches Verfahren für die Bestimmung von morphologischen Parametern und physiologischen Eigenschaften von Hautgewebe, wobei das Verfahren die folgenden Schritte umfasst:

Erzeugen von Reflexionsmessungen einer Hautgewebefläche aus Reflexionsbildern, die für eine Vielzahl von Wellenlängen aus mehreren Beleuchtungs- und Nachweiswinkeln unter Verwendung eines Spektralreflektometers erhalten werden, das aus einem Messkopf mit 12 fixierten Leuchtdiode (LED)-Lampen und 3 Kameras besteht, wobei jede LED-Lampe in einem unterschiedlichen Winkel in Bezug auf die Haut positioniert wird,
Bereitstellen eines bio-optischen Modells, eines Strahlungstransfermodells und eines nichtlinearen Inversionsverfahrens;
systematisches Variieren von Eingabewerten der morphologischen Parameter und physiologischen Eigenschaften des Hautgewebes und gleichzeitiges Variieren von inhärenten optischen Eigenschaften des Hautgewebes, wobei die inhärenten optischen Eigenschaften mit den morphologischen Parametern und den physiologischen Eigenschaften des Hautgewebes durch das bio-optische Modell verknüpft sind, und
Errechnen von Reflexionen durch das Strahlungstransfermodell für die variierenden inhärenten optischen Eigenschaften, bis eine Übereinstimmung zwischen den Reflexionsmessungen und den Reflexionen, die durch das Strahlungstransfermodell errechnet wurden, einen vorgegebenen Genauigkeitsgrad erreicht; und
Erhalten der morphologischen Parameter und der physiologischen Eigenschaften, die durch das nichtlineare Inversionsverfahren ausgegeben werden.

2. Verfahren nach Anspruch 1, wobei das bio-optische Modell auf aufgestellten Absorptions- und Transmissionsspektren für bekannte Hautgewebe-Chromophore beruht und morphologische Parameter und physiologische Eigenschaften von Gewebe mit inhärenten optischen Eigenschaften von Gewebe in Beziehung bringt.

3. Verfahren nach Anspruch 1, wobei das Strahlungstransfermodell in gekoppelten Luft-Gewebe-Systemen verwendet wird, um synthetische Reflexionsspektren für eine Vielzahl von unterschiedlichen Wellenlängen und eine Vielzahl von unterschiedlichen Messungskonfigurationen, jede mit vorgegebenen Beleuchtungs- und Beobachtungsrichtungen, zu errechnen.

4. Verfahren nach Anspruch 1, wobei das nichtlineare Inversionsverfahren auf einer Theorie optimaler Schätzung beruht, um das inverse Problem der Quantifizierung von vorgegebenen morphologischen Parametern und physiologischen Eigenschaften von Hautgewebe zu lösen, wobei die morphologischen Parameter und physiologischen Eigenschaften von Hautgewebe optional Folgendes einschließen: dermalen Blutgehalt, prozentuale Blutoxygenie-

rung, Dicke der oberen Epidermis, Dicke der unteren Epidermis, prozentuale obere Melanosomkonzentration, prozentuale untere Melanosomkonzentration und prozentuale Keratinkonzentration.

5. Verfahren nach Anspruch 1, wobei das Verfahren zur Unterscheidung zwischen einem von Folgenden verwendet wird:

benignen pigmentierten Läsionen und malignem Melanom;
benignem Gewebe und Basalzellkarzinom; und
benignem Gewebe und Plattenepithelkarzinom.

6. Verfahren nach Anspruch 1, wobei das Verfahren für die Schönheitspflege, Gerichtsmedizin oder zur Überwachung von Wirksamkeiten von unterschiedlichen Behandlungsarten verwendet wird.

Revendications

1. Procédé optique pour déterminer des paramètres morphologiques et des propriétés physiologiques de tissu cutané, le procédé comprenant les étapes :

de génération de mesures de réflectance d'une zone de tissu cutané à partir d'images de réflectance obtenues pour une pluralité de longueurs d'ondes depuis plusieurs angles d'illumination et de détection en utilisant un lecteur de réflectance spectrale constitué d'une tête de mesure avec 12 lampes à diodes électroluminescentes (DEL) fixes et 3 caméras, dans lequel chaque lampe DEL est placée à un angle différent par rapport à la peau, de fourniture d'un modèle bio-optique, d'un modèle de transfert radiatif, et d'une procédure d'inversion non-linéaire ;
de variation de manière systématique de valeurs d'entrées des paramètres morphologiques et des propriétés physiologiques du tissu cutané et de variation de manière simultanée des propriétés optiques inhérente du tissu cutané,
dans lequel les propriétés optiques inhérentes sont liées aux paramètres morphologiques et aux propriétés physiques du tissu cutané par le modèle bio-optique, et
de calcul de réflectances par le modèle de transfert radiatif pour les propriétés optiques inhérentes variant jusqu'à ce qu'un accord entre les mesures de réflectance et les réflectances calculées par le modèle de transfert radiatif atteignent un niveau prédéterminé de justesse ; et
d'obtention des paramètres morphologiques et des propriétés physiologiques renvoyés par la procédure d'inversion non linéaire.

2. Procédé selon la revendication 1, dans lequel le modèle bio-optique est basé sur des spectres d'absorption et de transmission établis pour des chromophores de tissu cutané connus et fait concorder des paramètres morphologiques et des propriétés physiologiques de tissu avec des propriétés optiques inhérentes de tissu.

3. Procédé selon la revendication 1, dans lequel le modèle de transfert radiatif est utilisé dans des systèmes couplés tissu-air pour calculer des spectres de réflectance synthétiques pour une pluralité de longueurs d'ondes différentes et une pluralité de configurations de mesures différentes, chacun ayant des directions spécifiées d'illumination et d'observation.

4. Procédé selon la revendication 1, dans lequel la procédure d'inversion non linéaire est basée sur une théorie d'estimation optimale pour résoudre le problème inverse de quantification de paramètres morphologiques et de propriétés physiologiques spécifiés de tissu cutané, les paramètres morphologiques et les propriétés physiologiques de tissu cutané incluant facultativement, la teneur en sang dermique, le pourcentage d'oxygénation du sang, l'épaisseur de l'épiderme supérieur, l'épaisseur de l'épiderme inférieur, le pourcentage de la concentration supérieure des mélanosomes, le pourcentage de la concentration inférieure des mélanosomes, et le pourcentage de la concentration de la kératine.

5. Procédé selon la revendication 1, dans lequel le procédé est utilisé pour faire la différence entre un élément parmi :

des lésions pigmentées bénignes et un mélanome malin ;
un tissu bénin et un carcinome à cellules basales ; et
un tissu bénin et un carcinome à cellules squameuses.

6. Procédé selon la revendication 1, dans lequel le procédé est utilisé pour les soins de beauté, la médecine légale, ou pour surveiller les efficacités de différents types de traitement.

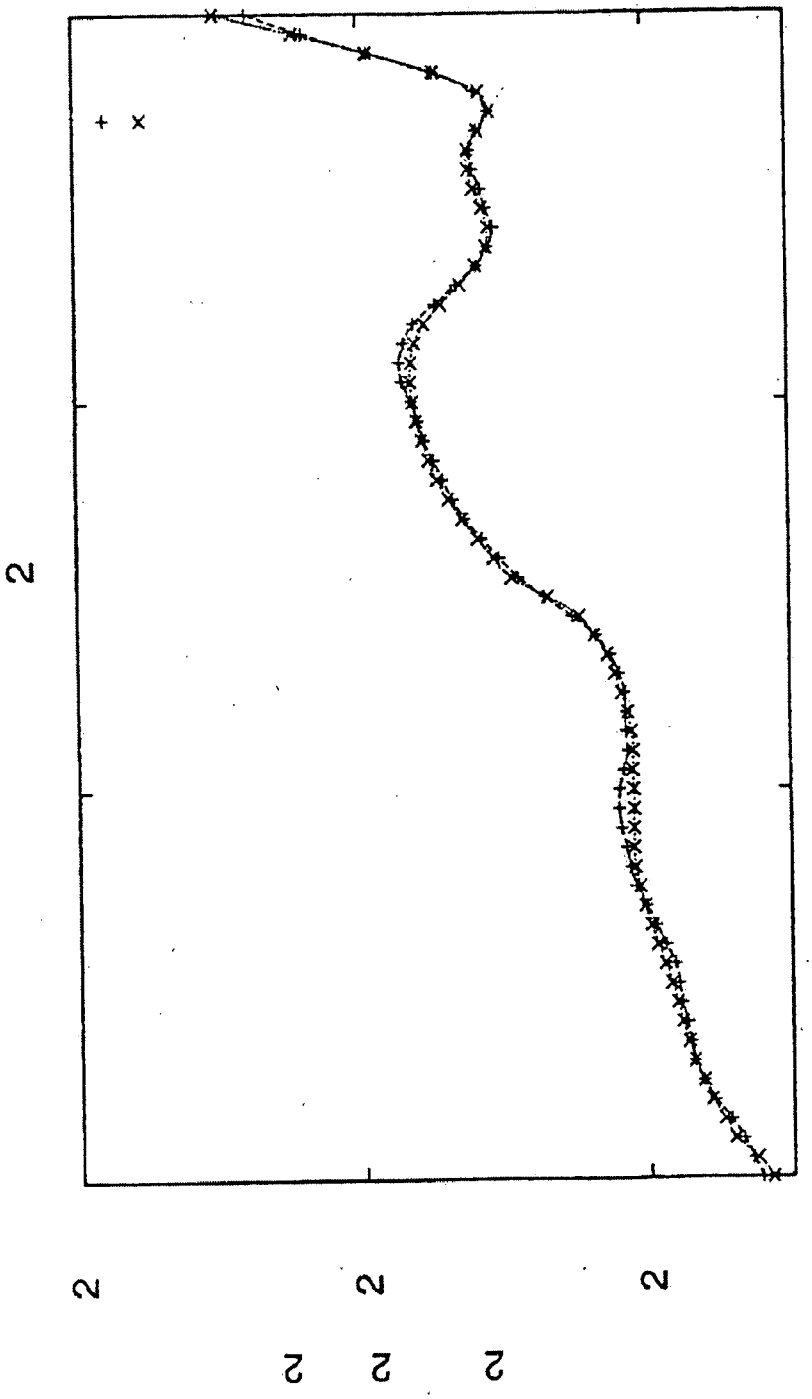

Figure 1

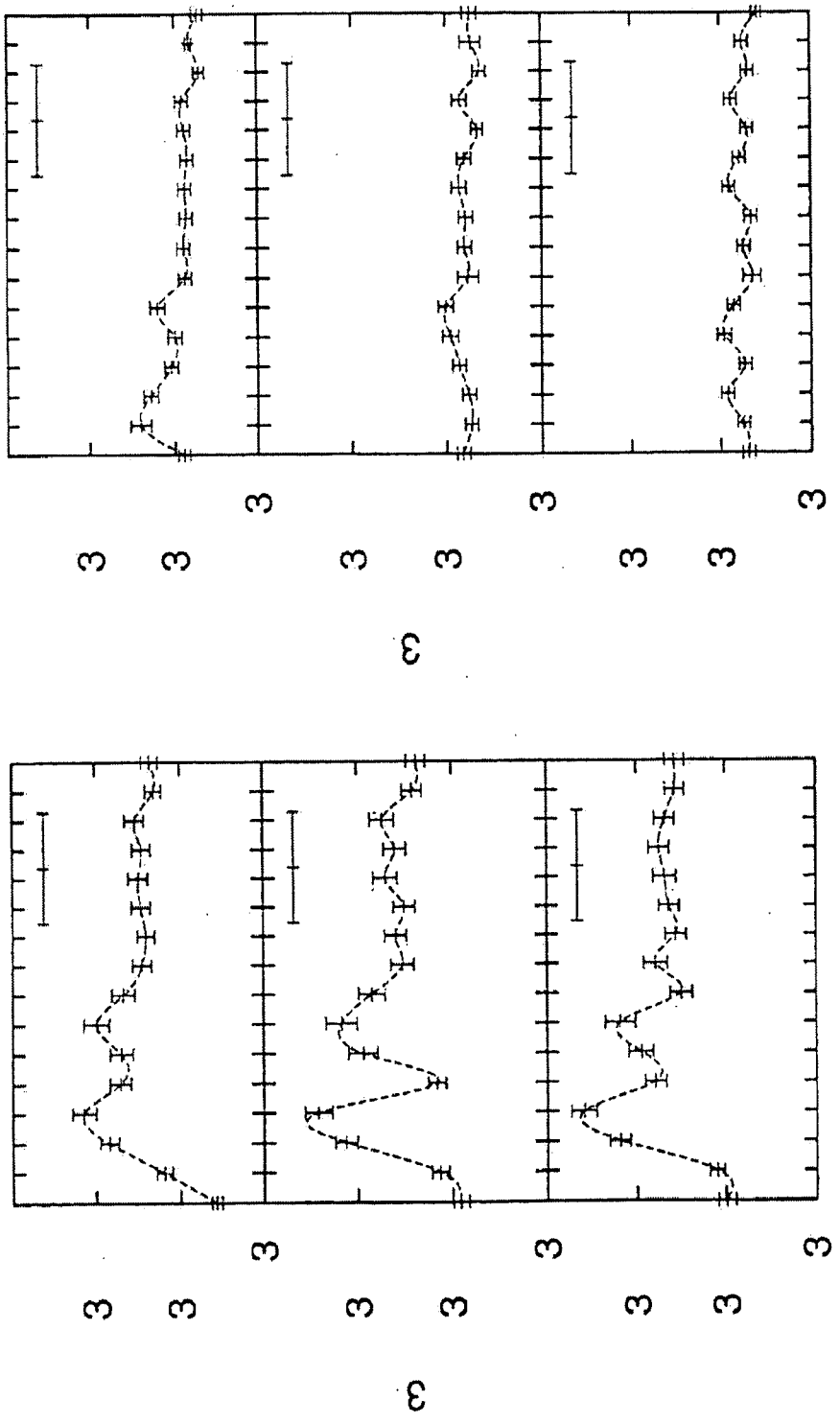

Figure 2

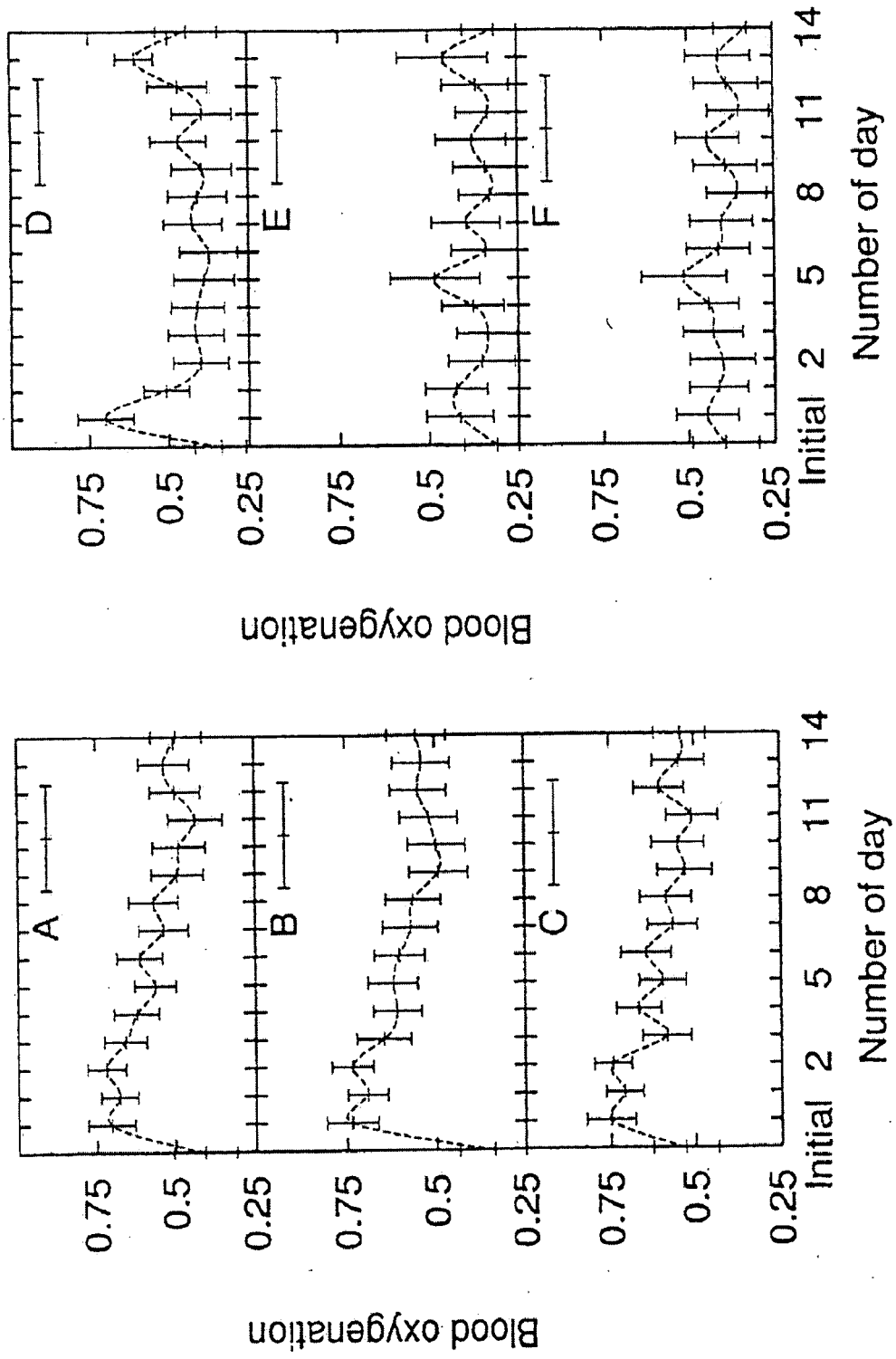
A
B
C
D
E
F
0.75
0.5
0.25
Initial
2
5
8
11
14
Number of day
Blood oxygenation

Figure 3

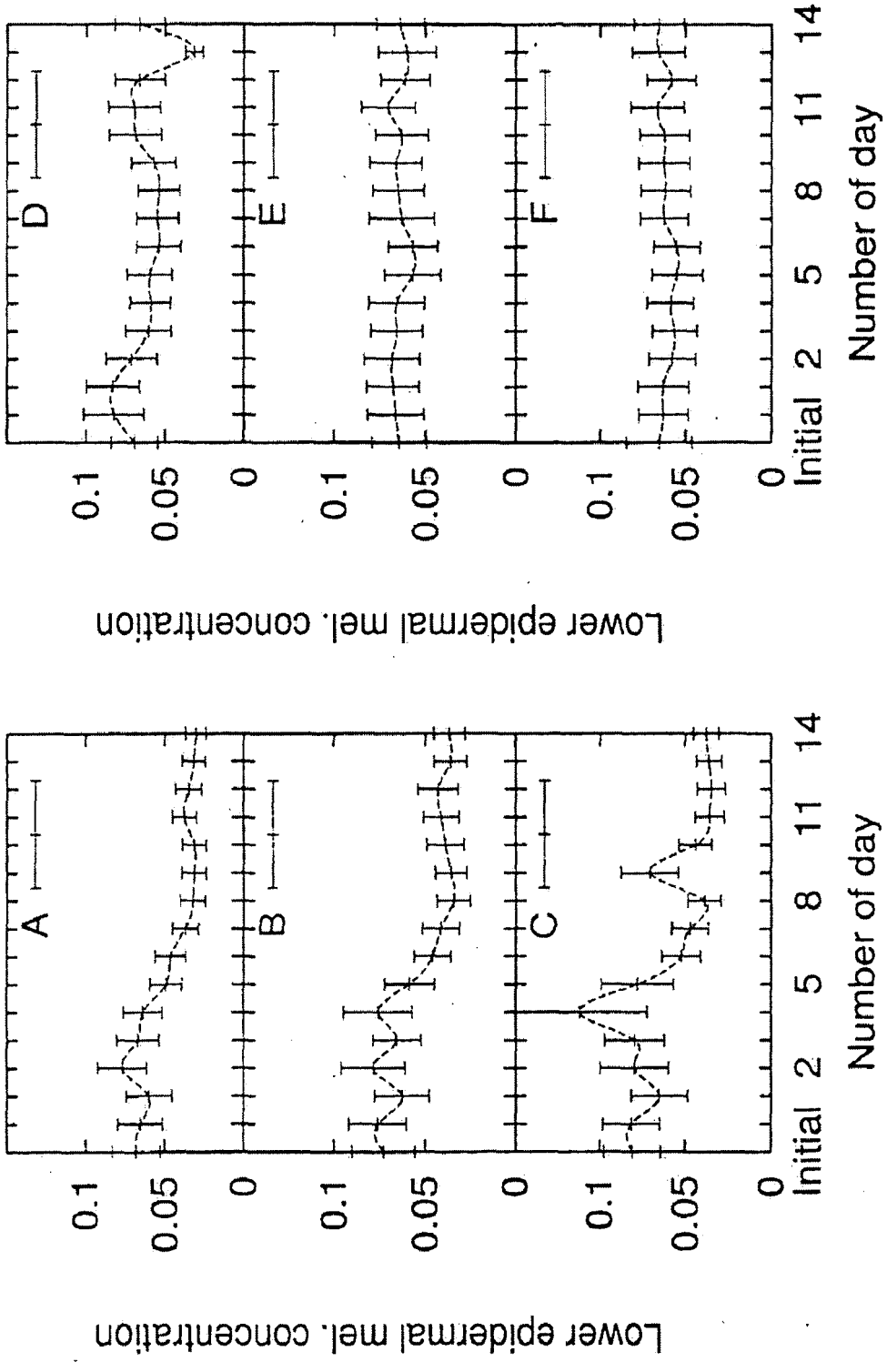
A
B
C
D
E
F
0.1
0.05
0
Initial
2
5
8
11
14
Number of day
Lower epidermal mel. concentration

Figure 4

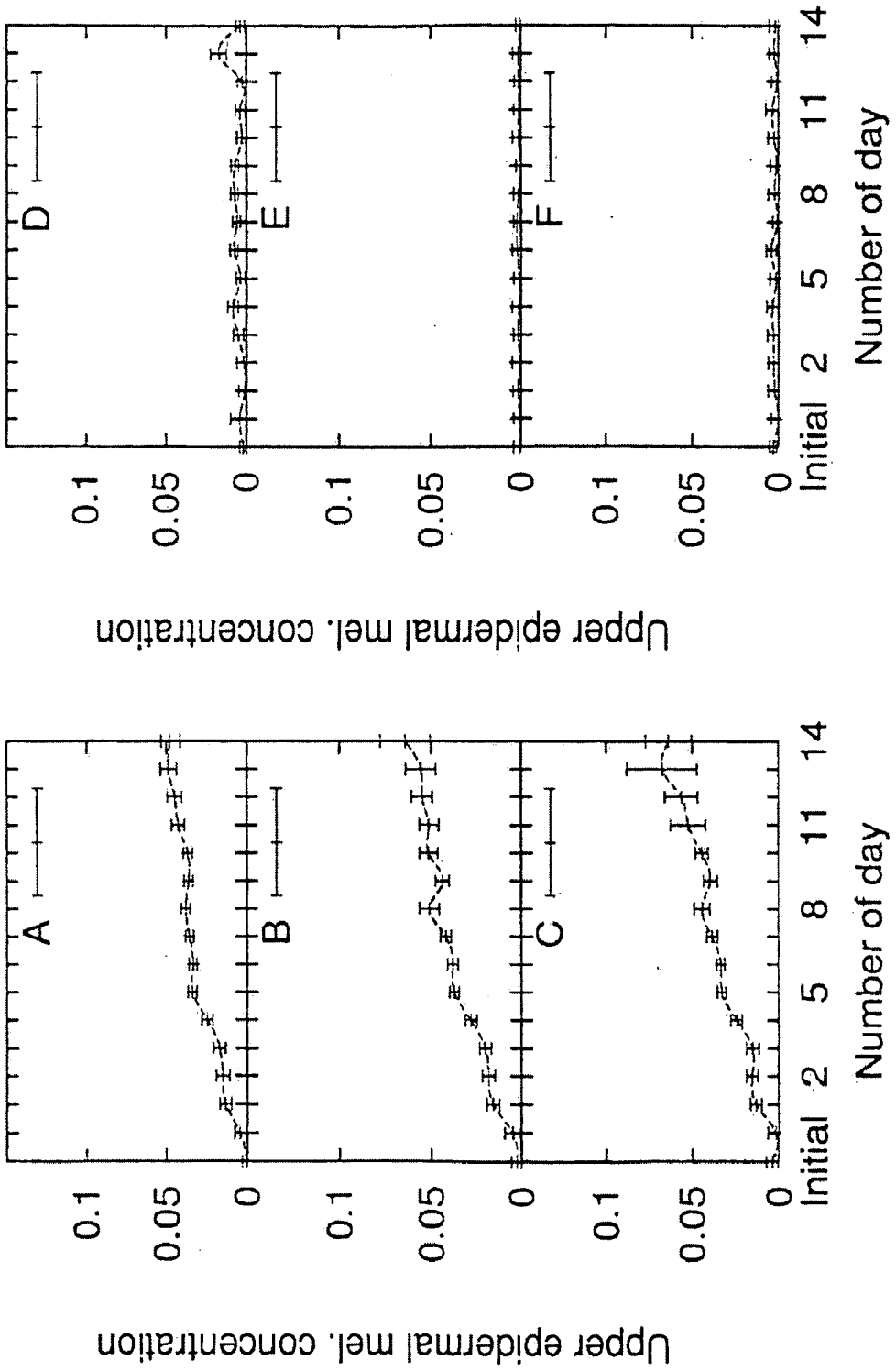
Upper epidermal mel. concentration
0.1
0.05
0
A
B
C
D
E
F
Initial 2 5 8 11 14
Number of day

Figure 5

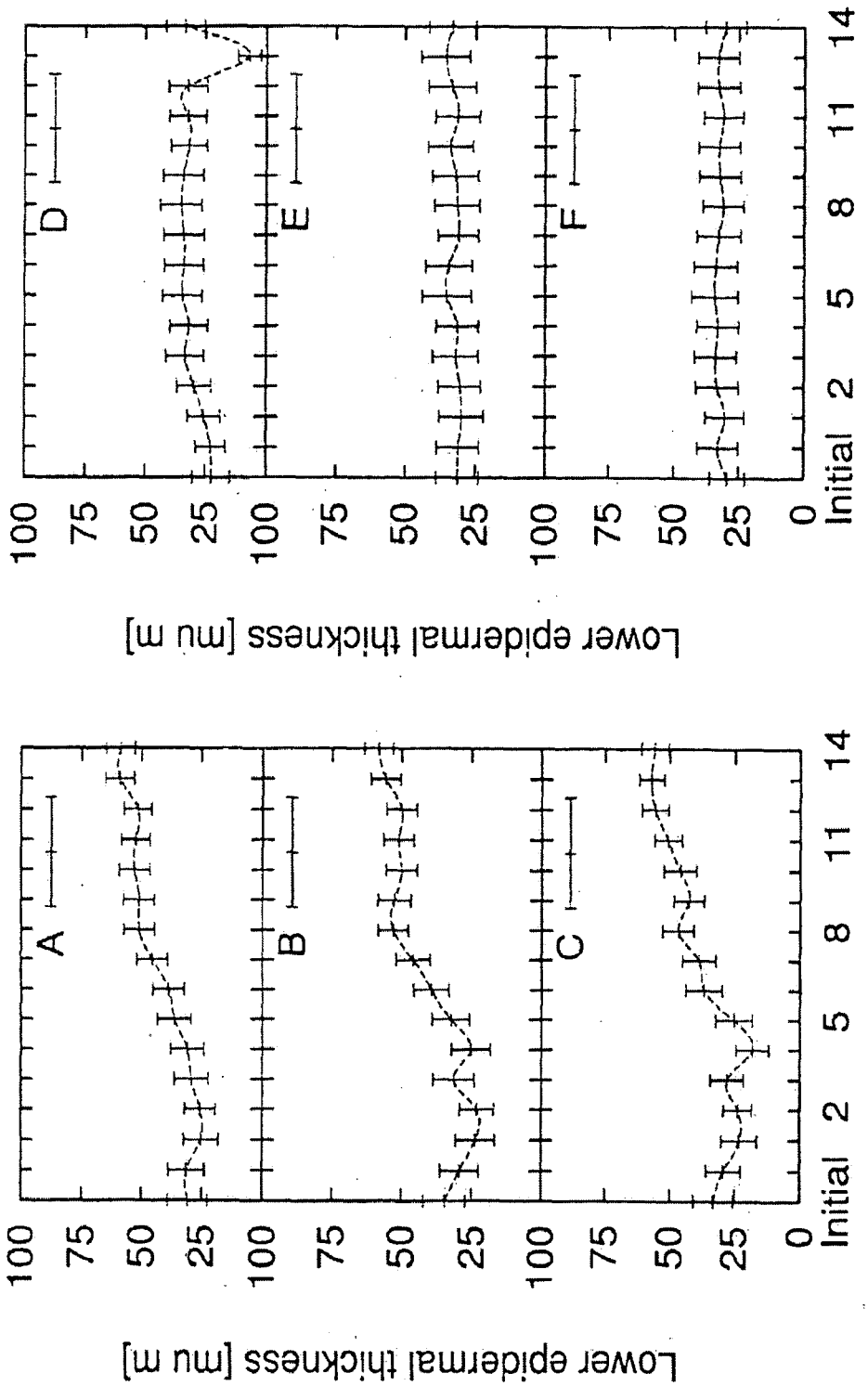
Lower epidermal thickness [mu m]
100
75
50
25
0
A
B
C
D
E
F
Initial
2
5
8
11
14
Number of day

Figure 6

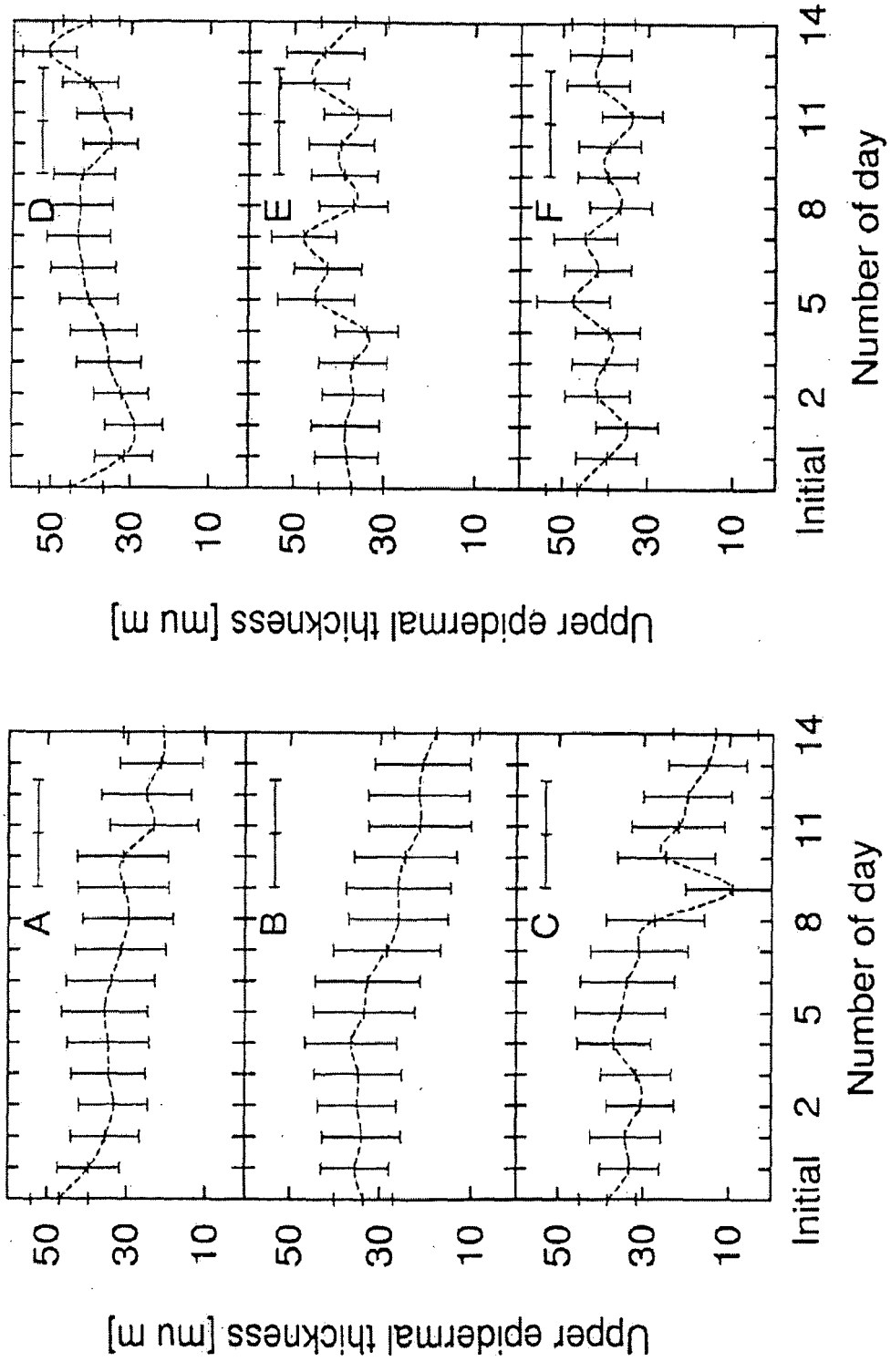
Upper epidermal thickness [mu m]
50
30
10
A
B
C
D
E
F
Initial
2
5
8
11
14
Number of day

Figure 7

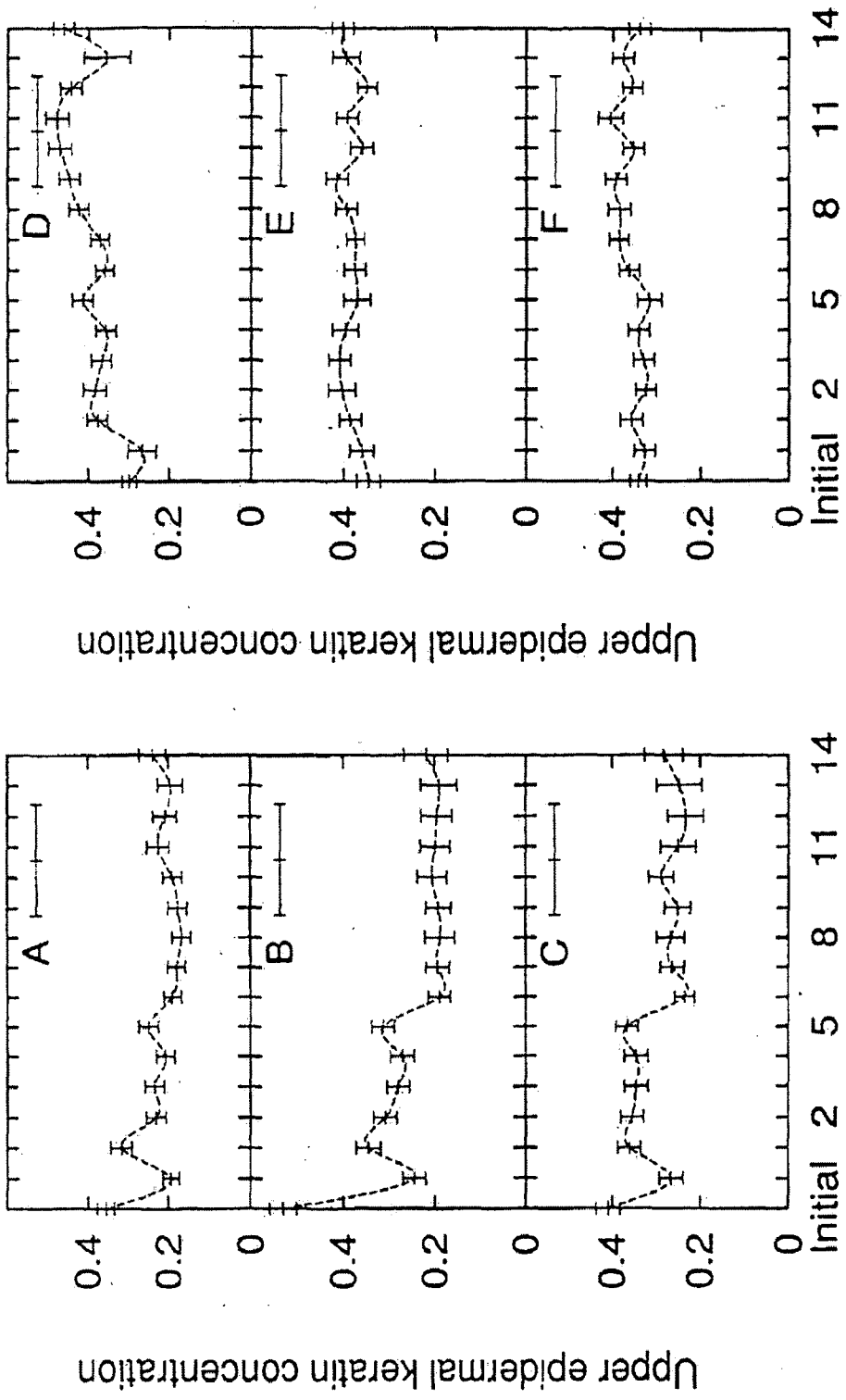
Upper epidermal keratin concentration
0.4
0.2
0
A
B
C
D
E
F
Initial 2 5 8 11 14
Number of day

Figure 8

REFERENCES CITED IN THE DESCRIPTION

This list of references cited by the applicant is for the reader's convenience only. It does not form part of the European patent document. Even though great care has been taken in compiling the references, errors or omissions cannot be excluded and the EPO disclaims all liability in this regard.

Patent documents cited in the description

- WO 2006076810 A1 **[0005]**
- US 2006247532 A1 **[0006]**

Non-patent literature cited in the description

- **HASSELBALCH, KA.** Quantitative Untersuchungen Uber die Absorption der menschlichen Haut von ultravioletten Strahlen. *Skand Arch Physiol,* 1911, vol. 25, 5-68 **[0003]**
- **EVERETT, MA ; YEARGERS, E ; SAYRE, RM ; OLSON, RL.** Penetration of epidermis by ultraviolet rays. *Photochem Photobiol,* 1966, vol. 5, 533-542 **[0003]**
- **DIFFEY, BL ; OLIVER, RJ ; FARR, PM.** A portable instrument for quantifying erythema induced by ultraviolet radiation. *Br J Dermatol,* 1984, vol. 111, 663-672 **[0003]**
- **YAROSLAVSKY AN ; SCHULZE PC et al.** Optical properties of selected native and human brain tissues in vitro in the visible and near infrared spectral range. *Physics in Medicine and Biology,* 2002, vol. 47 (12), 2059-2073 **[0003]**
- **KOLLIAS N ; BAQER AN.** Spectroscopic characteristics of human melanin in vivo. *J Invest Dermatol,* 1985, vol. 85, 38-42 **[0003]**
- **BERGER et al.** An enhanced algorithm for linear multivariate calibration. *Anal. Chem.,* 1998, vol. 70, 623-627 **[0004]**
- **KIENLE et al.** Spatially resolved absolute diffuse reflectance measurements for noninvasive determination of the optical scattering and absorption coefficients of biological tissue. *Appl. Opt.,* 1996, vol. 35, 2304-2314 **[0004]**
- **DAM et al.** Determination of tissue optical properties from diffuse reflectance profiles by multivariate calibration. *Appl Opt.,* 1998, vol. 37, 772-778 **[0004]**
- **ZHANG et al.** Neural vs. statistical classifier in conjunction with genetic algorithm based feature selection. *Pattern recognition letters,* 2005, vol. 26.7, 909-919 **[0004]**
- **TIKHONOV, A.N. ; ARSENIN, V.Y. ; TIKHONOV, A. N. ; V. Y. ARSENIN.** Solution of III-posed Problems. Winston & Sons, 1977 **[0004]**
- Introduction to the Mathematics of Inversion in Remote Sensing and Indirect Measurement Developments. **TWOMEY, S.** Geomathematics. Elsevier, 1977, vol. 3 **[0004]**
- **TARANTOLA, A.** Inverse Problem Theory: Methods for Data Fitting and Model Parameter Estimation. Elsevier, 1987 **[0004]**
- **RODGERS, CLIVE D.** Inverse Methods for Atmospheric Sounding: Theory and Practice. World Scientific, 2000 **[0004]**
- **NIELSEN KRISTIAN P. et al.** Reflectance Spectra of Pigmented and Nonpigmented Skin in the UV Spectral Region. *PHOTOCHEMISTRY AND PHOTOBIOLOGY,* 01 January 2004, vol. 80 (3 **[0007]**
- **NIELSEN KRISTIAN P. et al.** The optics of human skin: aspects important for human health. *SOLAR RADIATION AND HUMAN HEALTH,* 01 January 2008 **[0008]**
- **ZHAO, Y. ; BERNS, R. S.** Image-based spectral reflectance reconstruction using the matrix R method. *Color Res. Appl.,* 2007, vol. 32, 343-351 **[0030]**
- **SANDBY-MØLLER et al.** Epidermal Thickness at Different Body Sites: Relationship to Age, Gender, Pigmentation, Blood Content, Skin Type and Smoking Habits. *Acta Derm Venereol,* 2003, vol. 83, 410-413 **[0057]**

专利名称(译)	用于确定皮肤组织的形态参数和生理特性的光学方法		
公开(公告)号	EP2255173B1	公开(公告)日	2018-01-24
申请号	EP2009722309	申请日	2009-03-18
[标]申请(专利权)人(译)	巴尔特		
申请(专利权)人(译)	巴尔特INC.		
当前申请(专利权)人(译)	巴尔特INC.		
[标]发明人	STAMNES JAKOB J STAMNES KNUT ZHAO LU HAMRE BOERGE RYZHIKOV GENNADY BIRYULINA MARINA SOMMERSTEN ENDRE R NIELSEN KRISTIAN P MOAN JOHAN E		
发明人	STAMNES, JAKOB, J. STAMNES, KNUT ZHAO, LU HAMRE, BOERGE RYZHIKOV, GENNADY BIRYULINA, MARINA SOMMERSTEN, ENDRE, R. NIELSEN, KRISTIAN, P. MOAN, JOHAN, E.		
IPC分类号	A61B5/1455 A61B5/00 G01N21/47 G01N21/31 G06K9/00 G06T7/62 G06T7/66		
CPC分类号	A61B5/0059 A61B5/1455 A61B5/444 G01N21/4738 G06K9/00134 G06T7/62 G06T7/66 G06T2207/30024		
代理机构(译)	HANNA MOORE + CURLEY		
优先权	61/037503 2008-03-18 US		
其他公开文献	EP2255173A4 EP2255173A2		
外部链接	Espacenet		

摘要(译)

一种用于确定组织病变的形态参数的光学方法，包括：使用光学传递诊断装置产生病变的反射图像;并确定病变边界，病变的大小，直方图宽度，其给出病变的反射图像的不均匀性的度量，病变的相对惯性矩，中心距离表示几何中心之间的物理距离。病变和吸收质量中心，病变的分形维度，描述其边界的复杂性，病变的非球面性，病变的相对边界长度，以及可选地，病变的黑暗定义为病变反射强度的平均值。

$$\langle \cos\Theta \rangle = g = \frac{1}{2}\int_0^{\pi} p(\cos\Theta)\cos\Theta \sin\Theta \, d\Theta = \frac{1}{2}\int_{-1}^{1} p(\mu)\mu \, d\mu, \qquad (1)$$